RSC Advances

ROYAL SOCIETY OF CHEMISTRY

www.rsc.org/advances

RSC Advances

ARTICLE

Electrochemical Study of Nanoporous Gold Revealing Anti-Biofouling Properties

Received 00th January 20xx,
Accepted 00th January 20xx

DOI: 10.1039/x0xx00000x

www.rsc.org/

Shashank Saraf[a], Craig J. Neal[a], Sanghoon Park[b], Soumen Das[a], Swetha Barkam[a], Hyoung Jin Cho*[,b] and Sudipta Seal*[,a]

Nanoporous gold (NPG) has remarkable catalytic activity and biocompatibility and could potentially be used in biomedical devices. Herein, we have assessed the long term effects of biofouling on NPG interface. Nanoporoes (25 nm) in gold electrode are fabricated using a de-alloying treatment resulting in an 18 fold increase in surface area as compared to the planar gold. The effects of biofouling on the planar gold interface were evidenced by the rapid decrease in faradaic current to 55% in just eight minutes of incubation in 2 mg/ml of bovine serum albumin (BSA). On the other hand NPGshowed barely any decline in the peak current when incubated in a similar biofouling solution. NPG upon incubation in a solution of higher concentration of BSA showed immediate peak current degradation which was subsequently recovered when the electrode was left idle in the biofouling solution. For instance, the peak current regenerated from (60% to 80%) when left idle for 60 minutes in 16 mg/ml of BSA solution. The regeneration mechanism indicated that even after long term incubation in the biofouling solution, the accumulated organic layer on its interface is not impervious and allows the diffusion of small analytes molecules. Thereby, NPG could be used in biomedical devices such as biosensor or drug reservoir.

1. Introduction

Biological devices operate in an environment naturally comprised of innumerate organic molecules such as proteins, lipids, polysaccharides, nucleotides, etc. Operation inside the biomolecular milieu makes these devices especially prone to biofouling. Biofouling refers to the accumulation of these organic molecules on the surface of devices and resulting in the loss of functionality. For instance, an implanted device can develop 0.5-9 µm thick layer of accumulated biomolecules in just 21 days post implantation.[1] Foreign body reactions can be initiated by cytokine adsorption to the device's surface: leading to macrophage activation and production of fibroblasts that crosslink to form a collagenous, fibrous capsule.[2] This fibrous capsule inhibits diffusion of analytes to the implanted device rendering it inoperable.[3] Biofouling is also prevalent in in-vitro systems and results in sensor drift, loss of sensitivity, and the need for frequent recalibration.

In response, researchers have adopted several techniques which either inhibit or attenuate protein adsorption to rectify the mass transfer problems associated with biofouling. These approaches have involved chemical modification of surfaces, size selective exclusion of biomolecules using a porous membrane, modifying the topography of the device, etc.[4] In chemical modification, the device is coated with an ordered organic layer also known as a self-assembled monolayer (SAM).[5] This approach is a popular solution due to its inherent simplicity as well as to the versatility afforded by the variety of usable polymer species. The SAM layer functions as a physical/chemical barrier preventing adsorption of protein, while allowing electron transfer to the underlying, sensing electrode. However this approach limits the operating environment of the device and is quite sensitive to precipitous changes in pH or redox potential through desorption of the SAM layer.[5] Additionally displacement of SAM molecules can occur due to competitive adsorption from organic species in the physiological environment leading to degradation of the SAM layer.[6] Another approach is centered upon the use of size selective membrane such as nafion based porous membrane which, in other studies, have shown an effective way to reduce biofouling by excluding particular biomolecules.[7] The membranes showed excellent protection in short term use. However, it suffers from mineralization, leading to stress cracking from protein adsorption in prolonged exposure.[8] More recently, the selective permeability of silicon nanoporous membranes were used to prevent biofouling.[9, 10] These did not suffer mineralization and could therefore be used for longer periods of time. However, addition of these extra features to electrodes, when sensing and actuation is needed, involves incorporation of additional complexity into device fabrication. We have incorporated the concept of nanopores into the use of gold electrodes and successfully

[a] Advanced Materials Processing and Analysis Center (AMPAC), Materials Science Engineering (MSE), NanoScience Technology Center (NSTC), College of Medicine, University of Central Florida, 4000, Central Florida Boulevard, Orlando, FL 32816, USA.
[b] Department of Mechanical and Aerospace Engineering, University of Central Florida, 4000, Central Florida Boulevard, Orlando, FL 32816, USA

demonstrated that a nanoporous gold (NPG) sensing electrode could still acquire amperometric signals in biofouling conditions.[11] Another study showed that nanoporoses in gold prevented the protein from getting inside pore cavities while allowing diffusion of small analyte molecules; thus generating redox signal.[12]

NPG has shown remarkable catalytic activities and has already been implemented in chemical sensing. It has been established that NPG acts as a catalyst in the reduction of oxygen and hydrogen peroxide in both aqueous and gas phase.[13-16] The cathodic current on NPG as compared to a planar gold surface was 14-times higher upon reduction of peroxide species.[17] Based on these results, enzyme free detection of peroxide by NPG has been reported.[14] Along with its use as an electrochemical biosensor, it has also been used as an immunosensor as well. Its large surface area to mass ratio was utilized to load higher quantities of antibodies which enabled picogram detection of cancer biomarkers.[18] Recently, NPG was shown to have potential for use in drug reservoirs and was demonstrated to release analytes over several weeks.[19]

Another advantage in using NPG is its relatively straightforward fabrication process and its direct use as an electrode without any additional treatment steps. It is typically fabricated using a dealloying treatment wherein an alloy of gold and silver is deposited followed by selective etching of silver.[20] The removal of silver from the gold matrix leaves behind a network of nanoporosities. The curvature in the nanoporosities results in a high density of atomic steps and kinks.[21] This atomic structure resembles that seen in catalytically active 3–5 nm gold nanoparticles and is the underlying reason behind its catalytic abilities. [21] Additionally an enhancement in signal is expected from nano-confinement effect wherein reactant molecules confined in nanopores, resulting in augmented frequency of collisions with the electrode surface. Thus, NPG could be used in various biological devices such as biosensor, drug delivery reservoirs, etc.. In this manuscript, we have studied and evaluated its susceptibility to biofouling in physiological concentrations of albumin. Albumin was chosen due to its relatively high abundance in blood (typically 35 to 50 mg/mL), strong surface charge, and its comparatively large overall size. A ferri/ferro redox probe was selected to study the available surface area and the diffusion of small sized molecules in NPG nanoporosities in the presence of a biofouling layer. This study shows that NPG was successfully able to generate faradaic current signals when incubated in a protein solution.

2. Results

2.1. Morphology, surface chemistry and area characterization of planar gold and NPG:

The fabrication of planar gold is achieved using the e-beam evaporation of gold on silicon. A gold and silver alloy is then electrochemically deposited and silver is subsequently etched out to form nanoporosities in the remaining gold layer. SEM images of NPG after the etching treatment are shown in **figure 1a**, and the inset shows a magnified version of the ligaments in the NPG. The SEM images of NPG display gold clusters 800nm in size separated by micro-scale cracks. These cracks are a common feature associated with the de-alloying treatment.[22] The pore size distribution curve shown in **figure 1b** calculated for over 50 data points, indicates a mean pore size of around 25 nm. Here, pore size defined as the shortest distance between neighbouring gold ligaments.

Apart from the morphological characterization, the surface chemical composition of NPG i.e. the atomic ratio of silver to gold (X=Ag:Au), is computed before and after the de- alloying treatment. Surface chemical composition is an important parameter governing the morphology and quantities of nanopores and will also aid in attaining reproducibility for the fabrication of the NPG electrode.[20] The atomic ratio is computed from XPS spectra which were acquired before and after the etching treatment as shown in **figure 1c.** The peak centered at 90 eV corresponds to the Au(4f) binding energy and the peak in between 360 to 380 eV corresponds to Ag (3d) binding energy. Due to the etching treatment the peak intensity corresponding to Au(4f) has increased and decreased in case of Ag(3d). Relative atomic ratio is calculated from a detailed multiplex spectra of Au(4f) and Ag(3d) (data not shown). The computed atomic ratio (Au/Ag), before and after etching treatment are 6 and 0.214, respectively. This indicates a significant drop in the ratio; due to dealloying treatment with a low residual Ag content.

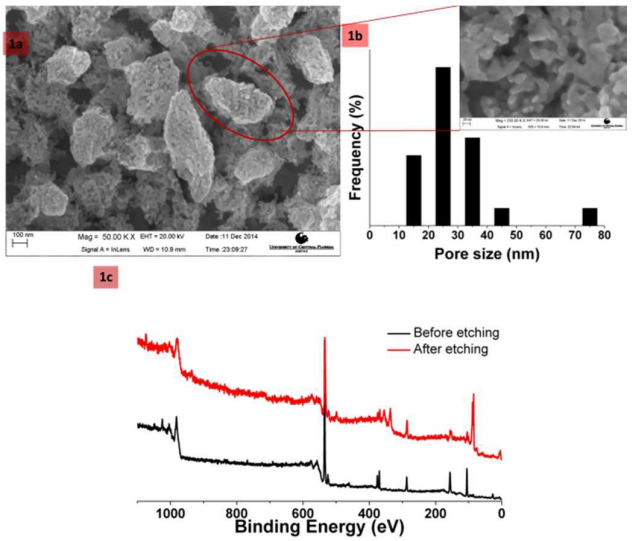

Figure 1 Shows the size and the surface chemistry characterization of NPG. Fig. 1a. shows the SEM image of the NPG electrode depicting the nanoporous structure in and its inset shows the high resolution image. Fig. 1b shows the size distribution of the nanopores measured from the SEM image. Fig. 1c showed the XPS spectra acquired before and after the etching process.

The geometric diameters of planar gold and nanoporous gold (NPG) are the same which are roughly 5 mm. However, the actual surface area of NPG is much larger than its geometric surface owing to a large network of nanoporosities. The actual surface area of NPG is typically obtained by computing the charge transfer resulting from the reduction of gold oxide (AuO) and describes the electrochemically active surface.[23]

This approach is most significant because it describes the electrode surface area via its electrochemical activity; resulting values describe an 'effective' surface area. Prior to surface area measurement, NPG was electrochemically cleaned using the procedure stated in experimental section. The electrochemical cleaning of gold is considered to yield the cleanest surface of any technique.[24] The consistency of cyclic voltammograms (CV) in subsequent cycles indicates a successful cleaning of the electrode. The surface area was then estimated from its CV curves in 10 mM H_2SO_4 solution where it exhibits Au oxidation and reduction peaks. The total charge transfer is obtained by integrating the peak corresponding to the gold reduction and the surface area is then estimated using the conversion parameter: 390μC/cm^2.[25] The surface area in the case of planar gold is expected to be same as its geometrical area. The CV curve of planar gold and NPG in 10 mM H_2SO_4 solution, as shown in **figure 2a**, shows peaks corresponding to the oxidation and reduction of Au. The peak located in the reverse sweep at 0.727 V and 0.835 V for planar gold and NPG respectively corresponds to the reduction of the gold oxide. The integrated charge density in the case of NPG was almost 18 times higher than that of planar gold indicating that the surface area of NPG is also 18 times higher than that of planar gold. Additionally, the peak current for the NPG electrode is almost 10 times higher than the planar gold electrode. Further, the CV curve is typical for a pure gold surface indicating that the residual Ag is not present at least on the surface of the electrode.

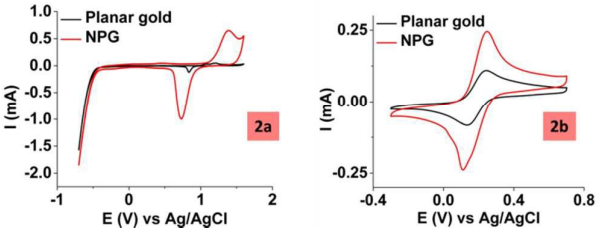

Figure 2a: CV of planar gold and NPG in 10 mM H2SO4 to estimate the electrochemical surface area. Figure 2b is the CV of both electrodes in presence of 10 mM ferri/ferro redox probe depicting a reversible behavior.

The cleanliness of planar gold and NPG was investigated prior to biofouling experiment by analyzing the redox behavior of ferrocyanide. It is widely reported that the ferri/ferro redox probe exhibits well-resolved cathodic and anodic peak current for gold electrodes through fast electron transfer kinetics. Following experimental CV, peak separation (ΔE_p) between the cathodic and anodic peak currents, resulting from the redox probe, is used to qualitatively express the cleanliness of the Au surface. Protein adsorption or general bio-fouling of the electrode will result in the decrease the peak current and increase the ΔE_p. Gold electrodes can also be contaminated by adsorption of organic impurities present in the testing environment.

The experimental CV of planar gold and NPG is acquired in 10mM potassium ferri/ferro cyanide, dissolved in 10mM phosphate-buffered saline (PBS) solution and is shown in **figure 2b**. The standard redox potential of KHCF is estimated by the following relation, which is later used as the working potential in the impedance spectroscopy experiment,

$$E^{o\prime} = \frac{E_{pa}+E_{pc}}{2} \quad (1)$$

The redox probe shows quasi-reversibility on NPG electrode as the ratio of cathodic to anodic peak current is 1.03 (ipc/ipa) and the peak separation (ΔEp) is approximately 0.100V (uncompensated). Additionally, the ratio between the cathodic peak current from NPG and planar gold electrode ($i_{pc}^{NPG}/i_{pc}^{Planar}$) is 1.1. On the other hand, the cathodic peak current ratio, corresponding to gold reduction in NPG and planar gold is approximately 10 as shown in **figure 2a**. The lower increase is attributed to the fast electron transfer kinetics in case of ferri/ferro redox probe resulting from the consumption of species on the top surface. This results in less penetration of ferro/ferri redox species into the nanoporous channels.[14] Thus, the peak current is dependent on the diffusion coefficient of the redox species. On the other hand, the peak patterns of gold oxidation and reduction are consistent with the slow transfer kinetics of surface confined redox species. Thus, the current is amplified by the higher surface area.

2.2. Planar gold and NPG response in Biofouling solution

In the laboratory, a biofouling environment is often simulated by using Human Serum Albumin (HSA) protein. It is the most abundant blood protein constituting nearly 50% of the total human blood plasma proteins. The typical physiological concentration of Albumin in human blood serum varies from 35 mg/ml to 50 mg/ml. In this study, Bovine Serum Albumin (BSA) which has a similar structure and similar properties as HSA, is selected as a model protein to systematically study the biofouling in planar gold and NPG electrode. The electrodes biofouling resistance was initially tested by incubating them in BSA solution at a concentration of 2 mg/ml. The extent of biofouling on the electrodes is inferred from the charge transfer kinetics of the ferri/ferro redox probe. Any fouling on the electrode surface would lead to an increased degree of irreversibility and slow electron kinetics.[23] Therefore, the CV curves were acquired continuously for up to 50 minutes after the electrodes were immersed in BSA solution; shown in **figure 3a** and **figure 3b**. **Figure 3c** shows the resulting peak currents with rapid degradation in the case of planar gold while no change in peak current was observed for NPG. The peak current in planar gold has reduced to 55% of its initial value within 7.5 minutes of incubation. The peak potential separation also increased, as shown in fig. 3d, indicating a growing charge transfer resistance. Thus, the accumulation of BSA at the planar gold interface is increasingly blocking the surface; leading to higher charge transfer resistance. On the other hand, the biofouling in NPG over the same duration did not exhibit any decrease in the peak current **(fig. 3c)**. Based on these promising results NPG was further tested in higher concentrations of BSA.

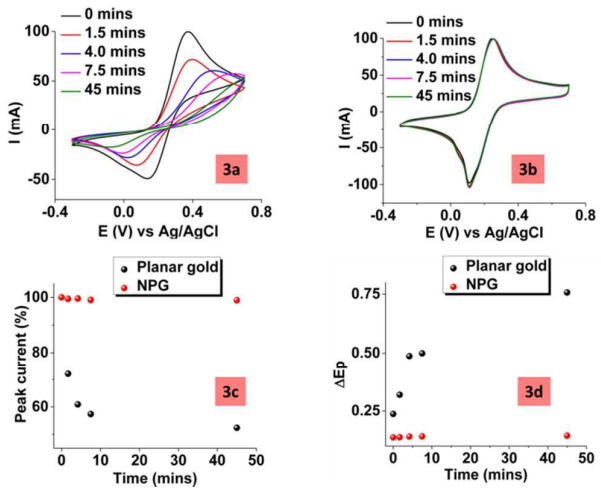

Figure 3: CV of the planar gold and NPG electrodes in 2 mg/ml BSA solution. Figure 3a shows the CV of planar gold electrode demonstrating the continual degradation of the peak current and within 8 minutes the redox current was indistinguishable from the background current. Figure 3b shows the CV of NPG electrode which did not show almost constant peak current over the time. Figure 3c shows the peak current as a function of time. Figure 3d shows the peak separation as a function of time.

2.3. NPG response in higher concentration of BSA

Multiple NPG electrodes were fabricated using the same parameters and exhibited similar surface area. These electrodes were then incubated in different concentrations of BSA. Specifically, the concentrations of BSA were varied from 2 mg/ml to 35 mg/mL, increasing the magnitude of biofouling and CV curve were obtained using the ferri/ferro redox couple. NPG incubated in a BSA solution with concentrations of 2 and 8 mg/ml did not exhibit any loss of peak current (data not shown). However, at higher concentrations of BSA, such as 16 and 25 mg/ml, the peak current starts to degrade as shown in **figure 4a** and **4b**. The CV was conducted continuously for up to 45 minutes. The results indicate a trend of decreasing peak current with time and becoming more pronounced as the concentration of BSA was increased. In 16 mg/ml the peak current reduced to 70% of its initial value in 15 mins of exposure to BSA. At the end of 45 minutes the peak current had decreased to ~60%. In the case of 25 mg/ml the peak current reduced to 60% in 15 mins of exposure and to 23% at the end of 45 mins. In the case of 35 mg/ml, which is not shown in the figure, the reduction of peak current happened very fast and it depreciated to 8% and 4% at the end of 15 and 45 mins, respectively, of exposure. In all cases the reduction in peak current is accompanied by an increasing peak separation, as shown in table 1, indicating an increasing degree of protein adsorption.

2.4. Regeneration of the peak current

An interesting phenomenon was noticed with longer incubation periods in BSA solutions. NPG started showing regeneration of the peak current after it had degraded. After leaving the NPG electrodes idle at the open circuit potential, in the biofouling solution, regeneration of the peak current happened in all cases of BSA concentration. BSA concentration and regeneration time shows a positive, proportional relationship. The CV demonstrating recovery of the peak current is shown in **figures 4c and 4d**. NPG in 16 mg/ml recovered 80% of its peak signal in just 400 minutes of idle time. When left idle overnight it regained 98% of its peak signal. In the case of 25 mg/ml the recovery was relatively slow and took ~50 hours to gain 96% of its peak current. In the case of 35 mg/ml the current recovered to 97% after 3 days had elapsed.

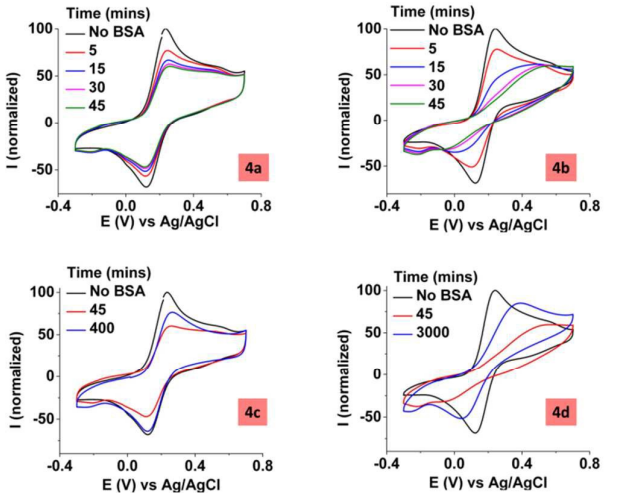

Figure 4: CV of NPG in different BSA concentration. Figure 4a and 4c shows the CV in 16 mg/ml of BSA. Figure 4b and 4d shows the CV in 25 mg/ml of BSA. Figure 4a and 4b shows the degrading peak current with time progression. Figure 4c and 4d shows the regeneration of the peak current.

Time [mins]	Planar gold-[2mg/ml]	NPG-[2mg/ml]	NPG-[16mg/ml]	NPG-[25mg/ml]
0	0.237	0.137	0.112	0.109
5	0.319	0.138	0.127	0.147
15	0.488	0.141	0.135	0.466
30	0.610	0.142	0.140	0.520
45	0.757	0.144	0.148	0.604

Table1: Increasing peak separation, ΔE (V) due to biofouling in planar gold and NPG electrode as function of incubation time in BSA solution

2.5. Electrochemical Impedance spectroscopy (EIS) on the electrodes

EIS was performed on planar gold and NPG at different incubation times in BSA solution to further investigate the biofouling features and the mechanism behind the regeneration of the peak current in NPG. In EIS an AC potential of varying frequencies is applied to the electrode. At higher frequencies the impedance of the system results from the electron transfer process and at lower frequencies it is governed by a diffusion limited process.[26] The data analysis gives valuable information about the protein layer adsorbed on the electrode ; specifically, illustrating the change in electron transfer kinetics due to due to biofouling on

electrodes[26-29]. Nyquist plots were obtained for electrochemically cleaned planar gold and NPG electrodes which were then immersed in BSA of concentration 2 mg/ml and 16 mg/ml respectively, along with 10 mM ferri/ferro redox probe. After incubation in BSA solution, electrodes were taken from solution and rinsed with de-ionized water to remove any un-adsorbed BSA species. Data was then acquired by dipping the electrode in PBS buffer solution containing the ferro/ferri redox probe. Nyquist plots as shown in **figures 5a and 5b**, were obtained to monitor changes in charge transfer resistance due to BSA adsorption on the electrodes. The electrodes were biased to the formal potential of the redox probe which was calculated from the cyclic voltammetry data using equation 1. Nyquist plot obtained for both planar gold and NPG electrodes prior to biofouling were fitted using the Randles circuit as shown in **figure 5e**. It is comprised of the following electrical components: R1 represents the electrolyte solution resistance (R1), CPE1 represents the constant phase element that models the capacitance associated with the electrical double layer, R3 represents the charge transfer resistance and Ws represents Warburg impedance is used to model the semi-infinite linear diffusion of the redox species. The charge transfer resistance in the case of planar gold was computed to be 850 Ω and 680 Ω in the case of NPG electrode.

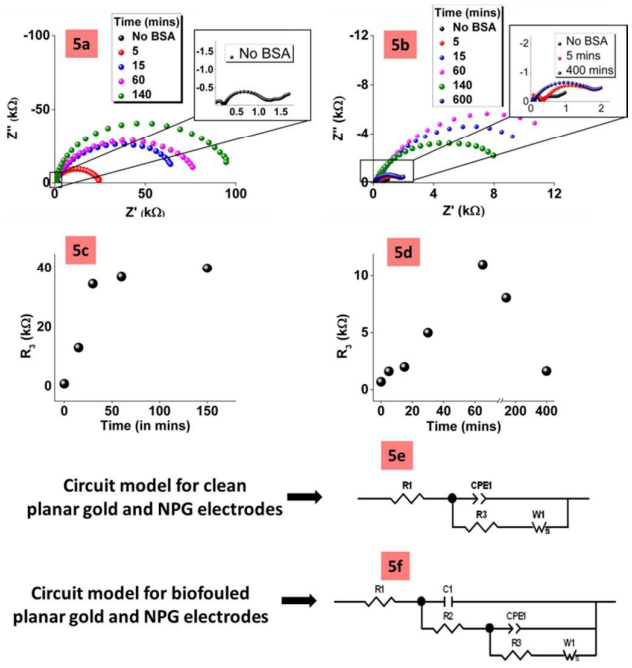

Figure 5: Nyquist plots of planar gold and NPG in biofouling solutions. Figure 5a shows the EIS spectra of planar gold in 2 mg/ml BSA showing continual increment in the impedance of the electrode. Figure 5b shows the EIS spectra of NPG in 16 mg/ml BSA solution, showing a decrease in the impedance after 140 minutes. Figure 5c and 5d denotes the trend in the circuit resistance element in case of planar gold and NPG respectively. Figure 5e and 5f shows the electrical circuit model used to fit the Nyquist plots corresponding to the clean electrodes and biofouled electrode.

Two additional parameters were added to the Randles circuit to modelling the Nyquist plots obtained from the electrodes which underwent biofouling as shown in **figure 5f**. These parameters are resistance (R2) and capacitance (C1) both corresponding to the adsorbed BSA film on the electrode surface.[29] Nyquist plots of planar gold and NPG after incubation in biofouling conditions for different durations, **figures 5c and 5d**. The diameter of the semicircles as seen in the Nyquist plots are a gives a rough measure of R3. In the case of the planar gold electrode, the diameter of the semicircle has increased exponentially indicating a similar trend in R3. While for NPG electrode, the diameter increased linearly up to 60 mins followed by a steep decline. The decrease in impedance after the idle time, corresponded with the recovery in the peak current as seen in the CV curves n **figure 4**. Another noticeable difference was seen in the absolute impedance values which were almost 10 times less for NPG as compared to planar gold.

The values of charge transfer resistance (R3) obtained through fitting are plotted as a function of time in **figures 5c and 5d** for planar gold and NPG respectively. In the case of planar gold the resistance increased steeply up until 60 minutes, followed by a slower rate of increase. It did not exhibit any decrease in the resistance magnitude. NPG on the other hand depicted a linear increase in the resistance which started to decrease after it was left idle for longer time periods in BSA solution. Peculiarly, after leaving NPG idle for periods long enough to obtain peak regeneration, the impedance of NPG became similar to the initial impedance response. The fitted value of R3 after 60 minutes was 11043 Ω which declined to 8063 Ω and 1638 Ω in 75 and 260 mins of idle time respectively.

2.6. Post regeneration electrochemical activity of NPG

The peak current in CV of NPG incubated in 16 mg/ml BSA solution after recovery showed a decline in peak current with successive cycles (**figure 6a**). The CV indicates that both anodic i_{pa} and cathodic i_{pc} peak current are decreasing, while the rate of declination is higher in the case of the anodic peak current. The ratio between anodic and cathodic peak current (X), for NPG before it was incubated in BSA solution remained consistent, around 1.1 (data not shown). The ratio signifies a higher anodic peak current over cathodic peak current for the ferri/ferro redox probe. This indicates a quasireversibility signifying less reduction of the oxidized species. Interestingly, the ratio just after incubation in BSA solution (16 mg/ml) showed a constant decay with successive cycles of CV experiment, as shown in **figure 6(b)**. The initial drop in the ratio might have resulted from a decrease in the available electrochemical surface area due to BSA adsorption. The faster declination of the anodic peak current as compared to the cathodic peak current, might have resulted from the outward diffusion of the oxidized species from nanopores, and slow inward diffusion owing to the BSA layer. After the regeneration of peak current, the ratio X was restored to its original value, obtained before biofouling. The recovery of the peak current can be ascribed to the saturation of nanopores with redox species during the idle time. When the CV experiment is repeated, it leads to faster degradation in the ratio X. This likely occurs from the faster diffusion of species outside the pores while the inward diffusion is sluggish, due to

accumulated BSA layer, resulting in slower replenishment of the ferri/ferro species.

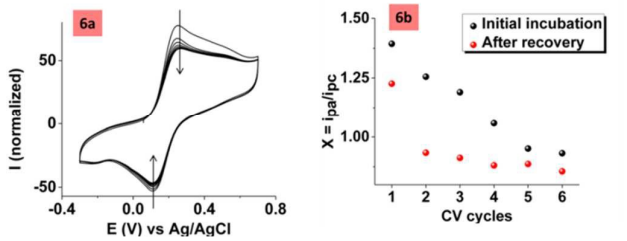

Figure 6: CV of the NPG electrode after the recovery of the faradaic current incubated in 16 mg/ml BSA. It shows the subsequent declination in the current with the progression of CV cycles. Figure 6b shows the ratio of anodic and cathodic peak current before and after the recovery. It shows the rapid declination of anodic peak current after the recovery phenomenon.

2.7. Release kinetics of fluorescein

The above mentioned experiments suggested that small sized molecules are able to diffuse through the adsorbed BSA layer. To substantiate this finding another experiment using a fluorescent molecule (fluorescein) was performed. A previous study showed that NPG could store these molecules in its nanopores and also studied its release kinetics in a PBS buffer solution.[19] Here the release kinetics will be affected, due to the adsorbed BSA layer. NPG was incubated in 2, 16 and 25 mg/ml concentrations of BSA. The results are shown in **figure 7**.

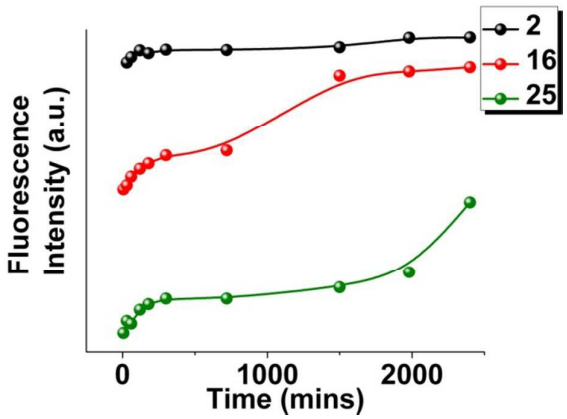

Figure 7: Shows the stacked fluorescence intensity of fluorescein as a function of incubation time in three different BSA solution of concentration 2 (black), 16 (red) and 25 (green) mg/ml

The figure shows a common feature of release kinetics: an initial burst release of fluorescein into the solution, common to all solutions of BSA. It is followed by different release kinetics behavior for all three BSA solutions. In 2 mg/ml the release was steady throughout the experimental duration. In 16 mg/ml release was delayed and jumped suddenly after ~1000 mins. Similarly, in case of 25 mg/ml a sudden increase in the release of fluorescein was observed at ~2000 mins. The results indicated a delayed release of fluorescein after an initial burst release due to the formation of an adsorbed BSA layer. The delayed release of fluorescein is similar to the response observed in the CV experiments originating from the diffusion barrier induced by the porous nature of the adsorbed layer.

3. Discussion

Planar gold and NPG were tested for biofouling resistance using cyclic voltammetry and impedance spectroscopy. The gold interface readily adsorbs BSA protein which results in the unfolding of BSA (denaturation) upon contact. The denaturation enables adsorption of multilayers of BSA through hydrophobic interactions of internal protein residues.[30, 31] In the case of planar gold, rapidly declining peak current in CV curves indicates a non-porous adsorbed BSA layer. NPG when incubated in same biofouling conditions as planar gold, demonstrates almost no loss of peak current which indicating a porous BSA layer. The porosity of the BSA layer might be due to its inability to enter the nanopores and forming a uniform film throughout the Nanoporous interface. The reason for this is twofold: similar dimension of nanopores and the BSA molecule and the double layer within the nanopores gives additional repulsive force to the like-charged, polarized BSA molecules. The phenomenon of double layer exclusion is widely reported in the case of nanostructured materials.[32] A thick, porous layer of BSA on NPG is expected as a result of the incubation in higher concentrations of BSA and is reflected in the continual declination of the peak current. The multilayer adsorption of BSA explains the formation of thick film which appears to be non-porous due to the regeneration of the peak current.

The kinetics of peak current degradation when NPG is incubated in different concentrations of BSA can be seen in **figure 8a**. At first in the lower concentration of BSA, NPG did not show any peak current degradation, maintaining its signal throughout the incubated time period, which spanned longer than 24 hours. When NPG was tested in concentrations greater than 16 mg/ml it started to show time-dependent degradation in the peak current. The peak currents for BSA of concentrations of 16, 25 and 35 mg/ml are plotted against time in **figure 8a** and are best fitted using the exponential decay function:

$$i = i_o e^{-bt} \quad (2)$$

Where ""i" is peak current at time "t", "i_o" is the initial peak current and "b" is the decay coefficient. The decay coefficient follows an increasing trend with BSA concentration of 16, 25 and 35 mg/ml which are 0.011, 0.032 and 0.410 sec^{-1},respectively. The peak current is directly proportional to the square root of the diffusion coefficient of the ferri/ferro species as shown in **equation 3**.

$$ip = 2.69 * 10^5 n^{3/2} A C D^{1/2} n^{1/2} \quad (3)$$

The degradation of peak current in CV experiments can be attributed to the reduction in the diffusion coefficients of ferri/ferro species through the BSA film formed due to biofouling. The diffusion coefficient is assumed to have an inverse relationship with the accumulated BSA, Q; as shown in **equation 5**. Substituting **equation 3 and 4** results in the analytical expression shown in **equation 6** which represents the BSA film formation as a function of time. Thus it can be reasoned that the proportionate amount of BSA is increasing exponentially with coefficient which is twice the decay coefficient.

$$i \propto D^{1/2} \quad (4)$$

$$Q \propto \frac{1}{D} \quad (5)$$

$$Q \propto \frac{1}{i^2} \quad (6)$$

$$Q = Q_o e^{2bt} \quad (7)$$

Figure 8(b) shows the proportionate amount of BSA adsorbed on NPG incubated in different concentration of BSA, as calculated using **equation 7,** versus recovery time. Each tested solution shows a similar trend: validating the hypothesis of diffusion across the BSA layer. The recovery time period allows ferri/ferro ions to diffuse into the nanopores as evidenced by the cyclic voltammetry result which shows regeneration of the peak current after the NPG electrode was left idle in BSA solution. The necessary recovery time was greater for NPG incubated in higher concentration of BSA.

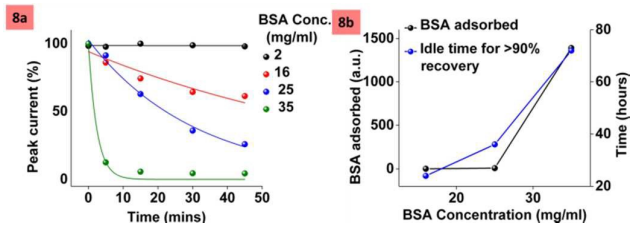

Figure 8: The anodic peak current in NPG incubated in different BSA concentration. All peak currents are normalized to the initial peak current when not incubated in BSA. Figure 8b shows the idle time required for NPG electrode to recover the peak current with analytically calculated amount of BSA adsorbed.

4. Conclusion:

The effect of biofouling on nanoporous gold interface is evaluated and compared to planar gold using the electrochemical response of ferri/ferro redox probe. Nanoporous gold is fabricated by a dealloying route yielding nanopores of average size 25 nm. The actual surface area of the NPG electrodes was 18 times higher than planar gold for the same geometrical area. Under the same biofouling conditions using BSA protein, Planar gold showed complete passivation of its interface while NPG maintained electrochemically active interface regions. For higher concentration of BSA pertaining to the physiological concentrations, biofouling protein formed a denser, porous multi-layer film and resulting in slower diffusion of ions through this film. Using an established analytical expression it was computed that the time required for the saturation of ions in the nanopores is directly proportional to the accumulated BSA. Therefore, NPG could be used in a biofouling environment and still allow the diffusion of smaller sized molecules. Due to this, NPG has a huge potential for use in biomedical devices. Potential applications include electrodes for biosensors, controlled drug delivery reservoirs, etc.

5. Experimental Section

5.1. Materials

Potassium dicyanoargentate (98%) and potassium dicyanoaurate (98%) were obtained from Sigma Aldrich and used as precursors to electrodeposit silver and gold respectively. Nitric acid (1N), sulfuric acid (70%), potassium iodide (99.5%), iodine (99.8%), potassium ferrocyanide (99.9%), and Bovine serum albumin (BSA) (>96%) were obtained from Sigma Aldrich for electrode etching and testing. Triple distilled water (>18 Mohms) is used wherever required.

5.2. Apparatus

Zeiss Ultra-55 scanning electron microscopy (SEM) and 5400 PHI ESCA X-ray photoelectron spectrometer (XPS) were used to characterize the gold electrodes. VSP model potentiostat from Bio-Logic Science Instruments was used to acquire cyclic voltammograms and impedance spectra. The potentiostat is equipped with built in EIS analyzer with frequencies ranging from 10 µHz to 1 MHz. Impedance spectra were fitted using the Z-View software. Fluorostar Omega, microplate reader was used to conduct the fluorescence studies.

5.3. Fabrication of planar gold and NPG

A thin film of 5 nm Ti and 150 nm Au was deposited on an oxidized silicon wafer by e-beam evaporation. Planar gold electrodes were made by the patterning gold coated wafer through UV photolithography and chemical etching of Au and Ti using Au etchant (20 g KI and 5 g I_2 in 200 ml DI water) in sequence. Electrodeposition of white gold and silver alloy onto these planar gold electrodes was carried out by immersing them in a solution composed of 10 mM potassium dicyanoargentate salt combined with a 10 mM solution of potassium dicyanoaurate salt in the volumetric ratio of 3:1 and applying current density of 3.7 mA/cm^2 for 20 minutes. Then nanoporous gold electrodes were fabricated through the de-alloying of the silver content in electrodeposited white gold layer by immersing the electrodes in concentrated nitric acid (70%) for 20 minutes.

5.4. Electrochemical testing

Cyclic voltammetry (CV) is used to electrochemically clean the electrode and in the analysis of the signal change due to biofouling of the electrode. A typical 3-electrode electrochemical setup composed of Ag/AgCl (saturated in 3M KCl) reference electrode, platinum mesh counter electrode and gold working electrodes was used throughout. All potentials were specified with regard to the reference electrode and were not compensated for solution resistance between the reference and working electrode. Prior to any measurements the gold electrode were electrochemically cleaned in 10 mM H_2SO_4 solution and performing CV between the potentials -0.3 to 1.6 V; at a scan rate of 100 mV/sec. An electrode was deemed cleaned when it showed consistent CV curves in subsequent cycles. The surface area of the electrode is estimated from the CV curves obtained in the same cleaning

solution. The CV curves corresponding to surface activity and cleanliness of electrodes are acquired in 10 mM $K_4[Fe(CN)]_6$ by cycling the potential between -0.3 to 0.7 V at a scan rate of 20 mV/sec. Electrochemical impedance spectroscopy (EIS) was performed in the frequencies ranging from 10 kHz to 100 mHz at the formal potential of the ferri/ferro redox couple as computed from the CV.

5.5. Release kinetics Fluorescein

NPG electrodes were first incubated for 1 hour in a 10 µM solution of 5-(and 6-)carboxy fluorescein, succinimidyl ester (Fluorescein) obtained from Fisher Scientific. Electrodes were then dried followed by incubation in BSA solution of different concentrations. The release kinetics of Fluorescein in the BSA solution were measured from the fluorescence intensity at 518 nm when excited at 494 nm

Acknowledgements

NSF EECS – 0901503 and partly NSF CBET-1261956 for nanotechnology/sensor research in biological environment.

Notes and references

1 1. P.-Y. J. Yeh, J. N. Kizhakkedathu, J. D. Madden and M. Chiao, *Colloids and Surfaces B: Biointerfaces*, 2007, **59**, 67-73.

2 2. S. Barkam, S. Saraf and S. Seal, *Wiley Interdisciplinary Reviews: Nanomedicine and Nanobiotechnology*, 2013, **5**, 544-568.

3 3. S. Vaddiraju, I. Tomazos, D. J. Burgess, F. C. Jain and F. Papadimitrakopoulos, *Biosensors and Bioelectronics*, 2010, **25**, 1553-1565.

4 4. A. Barfidokht and J. J. Gooding, *Electroanalysis*, 2014, **26**, 1182-1196.

5 5. N. K. Chaki and K. Vijayamohanan, *Biosensors and Bioelectronics*, 2002, **17**, 1-12.

6 6. J. C. Love, L. A. Estroff, J. K. Kriebel, R. G. Nuzzo and G. M. Whitesides, *Chemical reviews*, 2005, **105**, 1103-1170.

7 7. N. Wisniewski and M. Reichert, *Colloids and Surfaces B: Biointerfaces*, 2000, **18**, 197-219.

8 8. S. P. Adiga, C. Jin, L. A. Curtiss, N. A. Monteiro-Riviere and R. J. Narayan, *Wiley Interdisciplinary Reviews: Nanomedicine and Nanobiotechnology*, 2009, **1**, 568-581.

9 9. T. A. Desai, D. J. Hansford, L. Leoni, M. Essenpreis and M. Ferrari, *Biosensors and Bioelectronics*, 2000, **15**, 453-462.

10 10. L. A. Perelman, C. Pacholski, Y. Y. Li, M. S. VanNieuwenhze and M. J. Sailor, 2008, 3, 31-43.

11 11. D. Summerlot, A. Kumar, S. Das, L. Goldstein, S. Seal, D. Diaz and H. J. Cho, *Procedia Engineering*, 2011, **25**, 1457-1460.

12 12. J. Patel, L. Radhakrishnan, B. Zhao, B. Uppalapati, R. C. Daniels, K. R. Ward and M. M. Collinson, *Analytical chemistry*, 2013, **85**, 11610-11618.

13 13. R. Zeis, T. Lei, K. Sieradzki, J. Snyder and J. Erlebacher, *Journal of Catalysis*, 2008, **253**, 132-138.

14 14. F. Meng, X. Yan, J. Liu, J. Gu and Z. Zou, *Electrochimica Acta*, 2011, **56**, 4657-4662.

15 15. G. Yin, L. Xing, X.-J. Ma and J. Wan, *Chemical Papers*, 2014, **68**, 435-441.

16 16. J. H. Bae, J.-H. Han, D. Han and T. D. Chung, *Faraday discussions*, 2013, **164**, 361-376.

17 17. Y. Park and J. Kim, 2010, **13**, 251-255.

18 18. Q. Wei, Y. Zhao, C. Xu, D. Wu, Y. Cai, J. He, H. Li, B. Du and M. Yang, *Biosensors and Bioelectronics*, 2011, **26**, 3714-3718.

19 19. O. Kurtulus, P. Daggumati and E. Seker, *Nanoscale*, 2014, **6**, 7062-7071.

20 20. J. Erlebacher, M. J. Aziz, A. Karma, N. Dimitrov and K. Sieradzki, *Nature*, 2001, **410**, 450-453.

21 21. T. Fujita, P. Guan, K. McKenna, X. Lang, A. Hirata, L. Zhang, T. Tokunaga, S. Arai, Y. Yamamoto and N. Tanaka, *Nature materials*, 2012, **11**, 775-780.

22 22. Y. Ding, Y. J. Kim and J. Erlebacher, *Advanced materials*, 2004, **16**, 1897-1900.

23 23. F. Jia, C. Yu, Z. Ai and L. Zhang, *Chemistry of Materials*, 2007, **19**, 3648-3653.

24 24. L. M. Fischer, M. Tenje, A. R. Heiskanen, N. Masuda, J. Castillo, A. Bentien, J. Émneus, M. H. Jakobsen and A. Boisen, *Microelectronic engineering*, 2009, **86**, 1282-1285.

25 25. S. Trasatti and O. Petrii, *Pure and applied chemistry*, 1991, **63**, 711-734.

26 26. X. Chen, Y. Wang, J. Zhou, W. Yan, X. Li and J.-J. Zhu, *Analytical chemistry*, 2008, **80**, 2133-2140.

27 27. Q. Xie, C. Xiang, Y. Yuan, Y. Zhang, L. Nie and S. Yao, *Journal of colloid and interface science*, 2003, **262**, 107-115.

28 28. H. Heli, N. Sattarahmady, A. Jabbari, A. Moosavi-Movahedi, G. Hakimelahi and F.-Y. Tsai, *Journal of Electroanalytical Chemistry*, 2007, **610**, 67-74.

29 29. M. A. MacDonald and H. A. Andreas, *Electrochimica Acta*, 2014, **129**, 290-299.

30 30. K. Nakanishi, T. Sakiyama and K. Imamura, *Journal of Bioscience and Bioengineering*, 2001, **91**, 233-244.

31 31. S. H. Brewer, W. R. Glomm, M. C. Johnson, M. K. Knag and S. Franzen, *Langmuir*, 2005, **21**, 9303-9307.

32 32. S. Park, H. C. Kim and T. D. Chung, *Analyst*, 2012, **137**, 3891-3903.

33

RSC Advances

ARTICLE

Table of Contents:

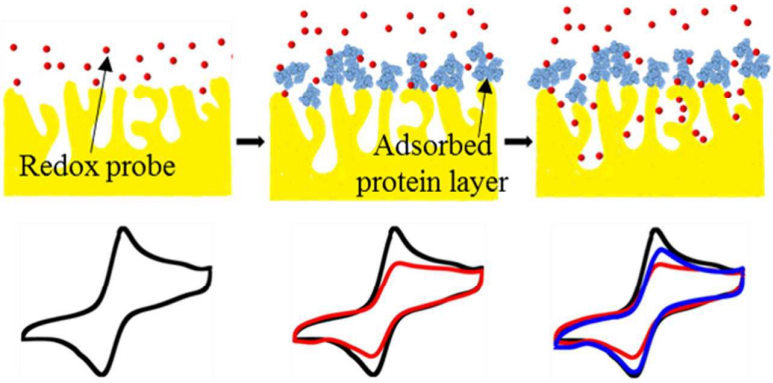

Schematic depicts the redox cycling on nanoporous gold as a function incubation time in biofouling solution. The adsorption of BSA protein depicts the porous morphology of the adsorbed layer on the nanoporous gold interface. Initial response of the biofouling resulted in the loss of faradaic current which again regenerated due to slow diffusion of the analytes through the fouled layer.